Tractable Modeling of Decision-dependent Customer Interruption Cost and Cold Load Pickup for Optimizing Power Distribution System Restoration

Wei Wang, Minwu Chen, Hongbin Wang, Gaoqiang Peng, and Hongzhou Chen

***Abstract*—Developing optimized restoration strategies for power distribution systems (PDSs) is critical to enhancing resilience. Prior knowledge of customer interruption cost (CIC) and load restoration behaviors, particularly cold load pickup (CLPU), is essential for effective decision-making. However, both CIC and CLPU are reciprocally influenced by the realized customer interruption duration (CID), making them decision-dependent and challenging to model, especially with limited understanding of underlying physical mechanisms. This study proposes a tractable modeling approach of decision-dependent CIC and CLPU for optimizing power distribution system restoration to capture the varying patterns of both CIC and CLPU with CID, i.e., patterns derived from data that reflect observable surface-level correlations rather than underlying mechanisms, thereby enabling practical surrogate modeling of decision-dependent factors. Specifically, quadratic functions are employed to model the increasing rate of CIC with respect to CID according to data fitting results. For CLPU, several defining characteristics are extracted and modeled in a piecewise linear form relative to CID, from which the actual restored load accounting for CLPU is subsequently reconstructed. Building on these models, a PDS restoration framework is developed, incorporating mobile energy storage systems (MESSs) and network reconfiguration strategies. Case studies validate the effectiveness of the proposed approach and highlight the unique potential of MESS in accelerating CLPU-related restoration.**

***Index Terms*—Restoration, power distribution system (PDS), customer interruption cost (CID), cold load pickup (CLPU), mobile energy storage system (MESS).**

Manuscript received: March 13, 2025; revised: August 5, 2025; accepted: October 12, 2025. Date of CrossCheck: October 12, 2025. Date of online publication: January 19, 2026.

This work was supported by the Fundamental Research Funds for the Central Universities, China (No. 2682025CX037).

W. Wang (corresponding author), M. Chen, and G. Peng are with the School of Electrical Engineering, Southwest Jiaotong University, Chengdu 611756, China (e-mail: ww0326@outlook.com; chenminwu@home.swjtu.edu.cn; 2023300247@my.swjtu.edu.cn).

H. Wang and H. Chen are with the Electric Power Research Institute, State Grid Chongqing Electric Power Company, Chongqing 401123, China (e-mail: whbleehomwhb@163.com; chz0617@foxmail.com).

DOI: 10.35833/MPCE.2025.000213

NOMENCLATURE

A. Sets

$\mathcal{K}_\alpha$, $\mathcal{K}_D$, $\mathcal{K}_t$	Sets of binary bit positions for decomposing $\alpha_{i,t}$, $D_{dc,i}$, and $t_{2,i}$
$\mathcal{L}_{out,t}$	Set of damaged branches during time span t
$\mathcal{M}$	Set of mobile energy storage systems (MESSs)
$\mathcal{N}_M$	Set of nodes accessible to MESSs
$\mathcal{N}$, $\mathcal{L}$	Sets of power nodes and branches of power distribution system
$\mathcal{N}_X$	Set of initially interrupted loads
$\mathcal{T}$	Set of time spans

B. Variables

$\alpha_{i,t}$	Integer variable indicating customer interruption duration (CID) for load i until the end of time span t
$\delta_{i,t}$	Binary variable indicating whether load i is restored during time span t
$\lambda^{(\alpha)}_{k,i,t}$, $\lambda^{(D)}_{k,i}$, $\lambda^{(t)}_{k,i}$	Auxiliary variables for decomposing $\alpha_{i,t}$, $D_{dc,i}$, and $t_{2,i}$
$\lambda_{ii',t}$, $\lambda_{i'i,t}$	Binary variables indicating whether arcs (i, i') and (i', i) are included in directed fictitious spanning tree during time span t
$\mu_{i'i,t}$	Binary variable indicating whether branch (i', i) is included in fictitious spanning tree during time span t
ξ_i	Binary variable indicating whether $D_{dc,i}\neq 0$
$A^{fun}_{i,t}$	Estimated increasing rate of customer interruption cost (CIC) for load i during time span t
$ch_{j,i,t}$, $dch_{j,i,t}$	Binary variables indicating whether MESS j charges and discharges at node i during time span t
$D_{pk,i}$, $D_{dc,i}$	Integer variables indicating peak and decay durations of cold load pickup (CLPU) for load i upon restoration
$d_{intr,i}$	Accumulated CID before restoration for load i

F_i	Peak magnitude of CLPU for load i upon restoration
$f_{ii',t}^{i_x}$, $f_{i'i,t}^{i_x}$	Directed flows of commodity i_x from nodes i to i' and nodes i' to i during time span t
Δf_i	Decay rate during CLPU for load i
$\kappa_{F,i}$, $\kappa_{pk,i}$, $\kappa_{dc,i}$	Binary variables indicating whether F_i, $D_{pk,i}$, and $D_{dc,i}$ is within segment prior to saturation
$P_{c,j,i,t}$, $P_{d,j,i,t}$	Active charging and discharging power of MESS j at node i during time span t
$P_{DG,i,t}$, $Q_{DG,i,t}$	Active and reactive power outputs of distributed generation unit at node i during time span t
$P_{IN,i,t}$, $Q_{IN,i,t}$	Active and reactive power injected by MESSs into node i during time span t
$P_{i'i,t}$, $Q_{i'i,t}$	Active and reactive power flows on branch (i', i) during time span t
$P_{L,i,t}$, $Q_{L,i,t}$	Actual active and reactive power of load i during time span t incorporating CLPU
$Q_{j,i,t}$	Reactive power of MESS j at node i during time span t
$soc_{j,t}$	State of charge of MESS j at the end of time span t
$t_{1,i}$, $t_{2,i}$, $t_{3,i}$	Timestamps for flagging CLPU process
$u_{1,i,t}$, $u_{2,i,t}$, $u_{3,i,t}$	Indicators for tracking CLPU process for load i during time span t
$v_{j,i,t}$	Binary variable indicating whether MESS j is traveling to node i during time span t
$V_{i,t}^2$, $V_{i',t}^2$	Squared voltage magnitudes at nodes i and i' during time span t
$\upsilon_{i'i,t}$	Binary variable indicating whether branch (i', i) of distribution system (DS) is closed during time span t
$x_{j,i,t}$	Binary variable indicating whether MESS j is parked at node i during time span t
$z_{k,i,t}^{(\sim)}$, $z_{k,i}^{(\sim)}$, $\beta_{i,t}$, $W_{\sim,i,t}$	Auxiliary variables for linearizing the bilinear terms

C. Parameters

ε_{pk}, ε_{dc}	Thresholds for rounding $D_{pk,i}$ and $D_{dc,i}$
$\alpha_{\max}$	An estimated maximum interruption duration
σ_1, σ_2, σ_3	Penalty coefficients for resource scheduling
η_i	Coefficient of power factor for load i
a_{i^*}, b_{i^*}, c_{i^*}	Quadratic coefficients for increasing rate of CIC versus interruption duration for load i^*, to which load i belongs
$a_{i,0}$	Interruption duration for load i preceding the scheduling
E_j	Energy capacity of MESS j
$e_{c,j}$, $e_{d,j}$	Charging and discharging efficiencies of MESS j
k_{F,i^*}, c_{F,i^*}, k_{pk,i^*}, c_{pk,i^*}, k_{dc,i^*}, c_{dc,i^*}	Linear coefficients for peak magnitude, peak duration, and decay duration of CLPU versus interruption duration for load i^*
M, ε	Large and small positive numbers
$p_{L,i,t}$	Original active power for load i during time span t
$P_{c,\max,j}$, $P_{d,\max,j}$	The maximum active charging and discharging power of MESS j
$P_{DG,\max,i}$, $Q_{DG,\max,i}$	The maximum active and reactive power outputs of distributed generation unit at node i
$Q_{\max,j}$	The maximum reactive power output of MESS j
$r_{i'i}$, $x_{i'i}$	Resistance and reactance of branch (i', i)
$soc_{j,\min}$, $soc_{j,\max}$	The minimum and maximum values of state of charge of MESS j
$S_{i'i}$, S_j, $S_{DG,i}$	Apparent power capacities of branch (i', i), MESS j, and distributed generation unit at node i
Δt	Length of unit time span
$V_{i,\min}$, $V_{i,\max}$	Lower and upper bounds of voltage magnitude at node i

I. Introduction

Enhancing the resilience of power distribution systems (PDSs) has become an urgent priority in both practice and research, driven by the rising frequency of extreme climate events and the global shift of many end-use energy demands toward electrification due to decarbonization efforts [1], [2]. A resilient PDS should, despite the various definitions of resilience, be well-prepared for disasters and capable of quickly restoring from them.

With specific regard to PDS restoration, recent decades have witnessed a surge in studies that build optimization models to explore the utilization of distributed energy resources (DERs) alongside network reconfiguration, forming microgrids with dynamic boundaries to quickly restore interrupted loads [3]-[5]. The flexibility of this process is particularly enhanced by incorporating the routing of mobile DERs, which include not only dedicated mobile energy storage systems (MESSs) and generators [6]-[8], but also electric buses and ships [9], [10]. However, despite existing innovative efforts, challenges persist in optimization modeling, particularly concerning decision-dependent factors.

Customer interruption cost (CIC) is undoubtedly a key component of the objective function, as it is crucial for prioritizing the sequence of load restoration and guiding the overall process. While significant attention has been paid to constraint modeling for the operation behaviors of emergency resources and PDS, far less consideration has been given to accurately representing CIC. Most studies incorporate a fixed CIC per unit time (e.g., in \$/kWh) into their objective functions, assuming that cumulative CIC (e.g., in \$/kW) increases linearly with customer interruption duration (CID) [11], [12]. However, customer surveys have revealed a nonlinear relationship between CIC (whether per unit time or cumulative) and CID [13]-[15], and the latter depends on the restoration decisions that need to be optimized. Obviously, accurate CIC is essential for making objective decisions on which loads to restore first during each time step, but this is challenging due to the lack of an analytical model linking CIC to CID; even if developed, such a model would likely be too complex to incorporate into optimization. Consequently, we are compelled to turn to representing CIC based on the limited statistical data we have, such as that from CIC surveys, i. e., an important pragmatic task for power utilities [16].

Beyond CIC, another critical decision-dependent factor is the restoration behavior of thermostatically-controlled loads (TCLs), known as the cold load pickup (CLPU) phenomenon, which is becoming increasingly significant with the growing penetration of TCLs in power systems driven by social development [17]. In many Chinese cities, air conditioning in summer has accounted for up to 60% of the peak load [18]. CLPU primarily stems from load inrush and the simultaneous start-up of numerous appliances due to loss of load diversity [19], with the latter being more prolonged and critical in restoration optimization [20]. It results in load surges beyond normal levels, characterized by factors such as peak magnitude, duration, and decay time, depending on elements including CID, ambient temperature, and load composition [19], [21]. While the latter can be accessed via situational awareness, CID remains undetermined until the optimal restoration decisions are made, making CLPU inherently decision-dependent. To ensure the effectiveness and feasibility of the final optimized decisions, we must first understand the extent of CLPU that will occur when restoring the interrupted loads at certain time. Therefore, it is essential to incorporate the relationship between CLPU and CID into the restoration optimized modeling process. However, similar to CIC, challenges exist due to the lack of a computationally tractable model for the relationship between CLPU and CID.

CLPU has long been on the radar of the power industry. For example, it is common to see that utilities issue notices for summer or winter outages, asking customers to unplug appliances after the power comes back to avoid potential failures induced by CLPU [22]. Nevertheless, studies aiming to quantitatively describe the relationship between CLPU and CID remain rather limited, let alone integrating it into restoration optimization. The classic study [23] provides handy formulas for peak magnitude and peak duration of CLPU; however, they come from heavy simplifications such as assuming identical thermostat settings and duty cycles across the entire customer population. Reference [24] derives a linear analytical relationship between CLPU magnitude and CID based on the operation characteristics of TCLs, which is then used to estimate the maximum recoverable load. Another phenomenon similar to CLPU in both mechanism and appearance is the energy rebound (or payback) following demand response (DR) events [25], which is mainly driven by the sudden and collective restart of devices after the DR ends. Reference [26] proposes a model for energy rebound and embeds it into a post-disaster PDS optimization framework. The model assumes that, within a fixed period after a DR event, the load rebounds by a certain proportion of the curtailed amount, e.g., 50% for commercial users and 100% for residential users, which is a commonly used assumption in this field [27]. This treatment implicitly accounts for the impact of CID on rebound magnitude. Overall, a few studies have explored the relationship between CID and CLPU or energy rebound, mostly focusing on the initial surge magnitude, rather than fully characterizing how CID influences the temporal behavior of CLPU. While [28] innovatively considers this impact by constructing a piecewise linear relationship between peak duration of CLPU and CID and integrating it into microgrid dispatch optimization, the CID-dependent variation of the decay process is not explicitly considered, despite being revealed in the study. Moreover, the impact of CID on peak magnitude of CLPU is not considered either.

Beyond these limitations in characterizing the relationship between CLPU and CID, a few studies have attempted to describe the TCL population behaviors from a probabilistic perspective, e. g., using approaches such as Fokker-Planck partial differential equations [29]. However, these approaches still rely on numerical solutions, making them hard to be embeded in optimization models. As a result, we are currently resorting to a data-driven approach, e.g., exhaustively accessing CLPU-related load data across all CID values via simulation or historical records, upon which we base the construction of the restoration optimization model [30]-[32]. However, the current approaches still face inherent limitations. First, simulation-based approaches require simulating the physical behaviors of TCL population across the full range of undetermined CID values over the restoration horizon. It is a daunting task, particularly when conducting precise simulation based on computational fluid dynamics (CFD), finite-element analysis, or specialized software like EnergyPlus™ [33]-[35], which, though high-fidelity, is computation-intensive. The enormity of this task is evident when attempting exhaustive pre-simulations across all CID values and environmental conditions like temperature, or even when deferred until restoration decisions are imminent (though other factors are clarified). Simulating across all CID values remains unavoidable, thus delaying critical decisions. In addition, for record-based approaches, ensuring records cover all CID values is prohibitively challenging due to monitoring limitations, infrequent blackouts, and difficulties with real-world outage experiments.

In light of the challenges in modeling either CIC or CLPU, the concept of data-driven optimization offers an insightful approach. The key idea in this emerging field is constructing surrogate models, also known as metamodels, to approximate objective or constraint functions that would otherwise have complex forms or require computation-intensive simulation or experiments [36], [37]. One major advantage is that these surrogate models can be trained on a limited amount of data, rather than requiring the entire dataset. This means we can be freed from the need for exhaustive simulation or records for each CID value, allowing restoration optimization to be carried out even with limited available CIC or CLPU data. In addition, the advantages also include the ability of well-trained surrogate models, e. g., through data fitting, to reduce the impact of data quality issues, such as noise or outliers [38], [39], thereby mitigating the overfitting risk that may arise when optimization is directly based on original data. Therefore, leveraging these insights, this study primarily focuses on building decision-dependent CIC model and CLPU model, which underpin the formulation of optimal PDS restoration problem. These models, though expressed in analytical form, do not represent the actual physical relationships between variables, but rather capture patterns present in the data. In other words, they are functions directly learned or fitted from data to characterize how CIC and CLPU change with CID, without trying to explain the internal physical causes. This is sufficient for restoration optimization, as it only requires the CID and CIC/CLPU mapping rather than the underlying full physical details. In this way, the complex and hard-to-derive physical mechanisms can be simply bypassed in the decision-making process. The specific contributions of this study are threefold as follows.

1) We characterize the decision dependency of CIC by defining it as the varying increasing rate of CIC with respect to CID. Based on the results of CIC and CID data fitting, quadratic functions are formulated to represent this dependency and then exactly linearized into tractable constraints.

2) The decision-dependent nature of CLPU is captured by extracting its varying characteristics with CID, including peak magnitude, peak duration, decay duration, and decay rate. These variations are modeled as piecewise linear functions, and the actual load accounting for CLPU is subsequently reconstructed based on these characteristics.

3) Based on the prior models, an optimization framework for PDS restoration is developed, integrating the scheduling of MESSs and network reconfiguration. The unique potential of MESSs to mitigate CLPU challenges is demonstrated through their capability of providing dynamic rating service across isolated islands, enabling short-term accommodation of CLPU-induced load surges and facilitating enhanced load restoration.

The rest of this study is organized as follows. Section II presents the modeling of decision-dependent CIC. Section III presents the modeling of decision-dependent CLPU. Section IV presents the modeling of PDS restoration optimization. Section V conducts case studies, and Section VI concludes this study.

II. Modeling of Decision-dependent CIC

A. Relationship Between CIC and CID

The electrical power industry has devoted decades to studying CIC via survey-based studies, with contributions from countries in North America and Europe [14], [15], [40]. A representative outcome is the ICE Calculator, which is a tool for CIC estimation and is developed based on extensive survey datasets and refined through multiple iterations. We used the ICE Calculator to conduct comprehensive testing, which was performed across a wide range of CID conditions, aiming to obtain sufficient CIC estimations. Subsequent fitting analysis uncovered a strong quadratic relationship between CID and the increasing rate of CIC, which has not been previously reported.

Figure 1 shows the estimated growth rates of CIC (marked by ×) under varying CIDs and the polynomial fitting results for different customers, where California is chosen as the region for estimation, with other parameters set as ICE Calculator defaults, such as household income and industry percentage. In Fig. 1, CI is short for commercial and industrial, and R^2 is the coefficient of determination, which is used to measure the goodness of fit of a model to the data, with the value range between 0 and 1. The closer the value is to 1, the better is the fitting performance.

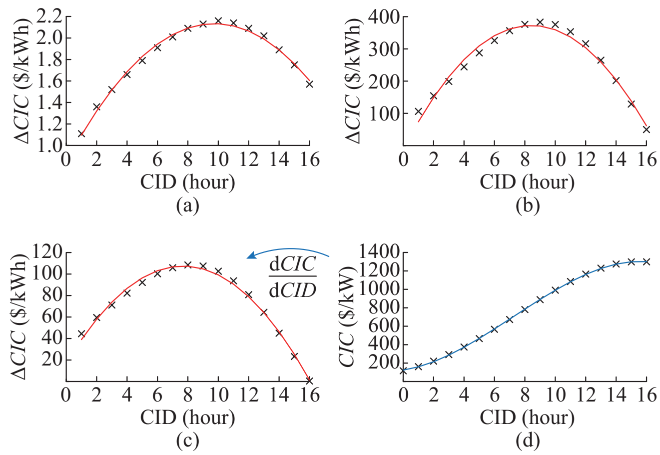

Fig. 1. Estimated growth rates of CIC under varying CIDs and polynomial fitting results for different customers. (a) Residential customer under $y=-0.0136x^2+0.2642x+0.8462$ and $R^2=0.9933$. (b) Small CI customer under $y=-5.4217x^2+91.3404x-11.7047$ and $R^2=0.9789$. (c) Large CI customer under $y=-1.5327x^2+23.5507x+17.0044$ and $R^2=0.9919$. (d) Cumulative CIC for large CI customer under $y=-0.5241x^3+11.4422x^2+24.6935x+123.5686$ and $R^2=0.9999$.

The quadratic relationship between the estimated increasing rate of CIC under varying CID, revealed by Fig. 1(a)-(c), suggests that after an 8-hour outage, the marginal cost of an additional hour is typically higher than that after 16-hour outage. This effect is even more pronounced for CI customers. Additionally, we also perform polynomial fitting on the generated cumulative CIC, showing a strong fit with a cubic function, as illustrated in Fig. 1(d). This further supports our findings, as the derivative of the cumulative CIC with CID directly corresponds to the growth rate. Although higher-order polynomials may offer a better fit, they often lead to overfitting and are generally discouraged in surrogate modeling for data-driven optimization [36]. In addition, they complicate conversion into tractable constraints, such as linear ones, as will be addressed subsequently.

B. Formulation of Linear Constraints

Even though the actual relationship between CIC and CID is complex, the data show that the relationship can be approximated using a quadratic function. Based on this approximation, we can build a surrogate model for the final optimization. First, we define $\alpha_{i,t}$ as a counter to track the CID that has already been experienced.

$$-M\delta_{i,t} \le \alpha_{i,t} - \left(\alpha_{i,t-1}+1\right) \le 0 \quad \forall i \in \mathcal{N}_X, \forall t \in \mathcal{T} \tag{1a}$$

$$0 \le \alpha_{i,t} \le \alpha_{\max}\left(1-\delta_{i,t}\right) \quad \forall i \in \mathcal{N}_X, \forall t \in \mathcal{T} \tag{1b}$$

Additionally, $\alpha_{i,0}$ is set as the initial CID for load i at the beginning of the current restoration horizon.

The growth rate of CIC, which follows a quadratic relationship with the ongoing interruption and drops to 0 upon restoration, can be explicitly expressed as:

$$A_{i,t}^{fun}=\begin{cases} a_{i^*}\left(\alpha_{i,t}\Delta t\right)^2+b_{i^*}\left(\alpha_{i,t}\Delta t\right)+c_{i^*} & \delta_{i,t}=0 \\ 0 & \delta_{i,t}=1 \end{cases} \tag{2}$$

This expression is further reformulated into the following constraints as:

$$0\le A_{i,t}^{fun}\le M\left(1-\delta_{i,t}\right) \quad \forall i\in\mathcal{N}_X, \forall t\in\mathcal{T} \tag{3a}$$

$$-M\delta_{i,t}\le A_{i,t}^{fun}-\left[a_{i^*}\left(\alpha_{i,t}\Delta t\right)^2+b_{i^*}\left(\alpha_{i,t}\Delta t\right)+c_{i^*}\right] \quad \forall i\in\mathcal{N}_X, \forall t\in\mathcal{T} \tag{3b}$$

$$\varepsilon-M\delta_{i,t}\le A_{i,t}^{fun} \quad \forall i\in\mathcal{N}_X, \forall t\in\mathcal{T} \tag{3c}$$

Particularly, as CID increases, the quadratic function may intersect the x-axis, as shown in Fig. 1(c) when CID exceeds 16 hours, leading to an unrealistic negative growth rate of CIC. In such cases, we set the rate to be 0, indicating that CIC no longer increases. Instead of introducing cumbersome binary variables to explicitly represent this piecewise function, we adopt a simpler approach facilitated by the optimization mechanism. We formulate (3b) and (3c) to enforce $A_{i,t}^{fun}$ to equal the greater value between the current CID-related functional CIC and ε when load i is interrupted, given that the objective function contains min $A_{i,t}^{fun}$. ε is a small positive number close to 0 but cannot be 0. If it is equal to 0, the load would not be restorable once its CID exceeds the intersection point.

Due to the negative a_{i*}, as shown in Fig. 1, (3b) is non-tractable due to non-convexity after linear programming (LP) relaxation, preventing its conversion to a tractable form like a second-order cone. Therefore, we replace $\alpha_{i,t}^2$ with $\beta_{i,t}$ and, given the integrality of $\alpha_{i,t}$, impose the following constraints (4a) - (4d) to guarantee the exactness of replacement [41].

$$\alpha_{i,t}=\sum_{k=0}^{\lfloor \log_2\alpha_{\max}\rfloor}2^k\lambda_{k,i,t}^{(\alpha)} \quad \forall i\in\mathcal{N}_X, \forall t\in\mathcal{T} \tag{4a}$$

$$-\alpha_{\max}\left(1-\lambda_{k,i,t}^{(\alpha)}\right)\le z_{k,i,t}^{(\lambda\alpha)}-\alpha_{i,t}\le 0 \quad \forall k\in\mathcal{K}_\alpha, \forall i\in\mathcal{N}_X, \forall t\in\mathcal{T} \tag{4b}$$

$$0\le z_{k,i,t}^{(\lambda\alpha)}\le\alpha_{\max}\lambda_{k,i,t}^{(\alpha)} \quad \forall k\in\mathcal{K}_\alpha, \forall i\in\mathcal{N}_X, \forall t\in\mathcal{T} \tag{4c}$$

$$\beta_{i,t}=\sum_{k=0}^{\lfloor \log_2\alpha_{\max}\rfloor}2^k z_{k,i,t}^{(\lambda\alpha)} \quad \forall i\in\mathcal{N}_X, \forall t\in\mathcal{T} \tag{4d}$$

Then, (3b) can be reformulated as:

$$-M\delta_{i,t}\le A_{i,t}^{fun}-\left(a_{i^*}(\Delta t)^2\beta_{i,t}+b_{i^*}\Delta t\alpha_{i,t}+c_{i^*}\right) \tag{5}$$

Additionally, the following constraints can be added as cuts to tighten the feasible region of the LP relaxation by forming McCormick envelops for the quadratic term $\alpha_{i,t}^2$, some parts of which are already implicit in (4).

$$\beta_{i,t}\ge 2\alpha_{\max}\alpha_{i,t}-\alpha_{\max}^2 \quad \forall i\in\mathcal{N}_X, \forall t\in\mathcal{T} \tag{6}$$

III. Modeling of Decision-dependent CLPU

A. Relationships Between CLPU Characteristics and CID

While the dependency of CLPU characteristics, e.g., peak magnitude, peak duration, and decay duration, on CID has gained attention, studies on quantitatively describing these patterns remain limited. Nevertheless, a few studies have attempted to approximate this dependency. For example, linear relationships between peak magnitude and CLPU peak duration with CID are derived in [23]. Though built upon multiple assumptions, such relationships are validated by recent studies [24], [28]. Since this study primarily focuses on mathematical and especially tractable modeling rather than directly examining the variation patterns of CLPU characteristics, we build on the foundation of these existing studies to support our work.

Specifically, we adopt a piecewise linear approximation for the CLPU curve [42] in Fig. 2(a). Compared with the traditional exponential decay model [20], [21], this approach tends to overestimate the extent of CLPU, providing an additional safety margin for the restoration process while also simplifying modeling and computation efforts. Three key characteristics are then selected to represent the CLPU process: peak magnitude, peak duration, and decay duration. Finally, we follow the evidence and data from [23], [24], and [28] and assume a two-stage linear relationship with saturation between CLPU characteristics and CID, as shown in Fig. 2(b). Based on this, we will derive constraints to form our model for CLPU. As new findings on the variation patterns of CLPU with CID emerge, the modeling process can be updated accordingly, e.g., by adopting a piecewise linear function with more segments in Fig. 2(b) to capture more complex patterns. Note that in Fig. 2, k_* and c_* denote the linear coefficients before saturation.

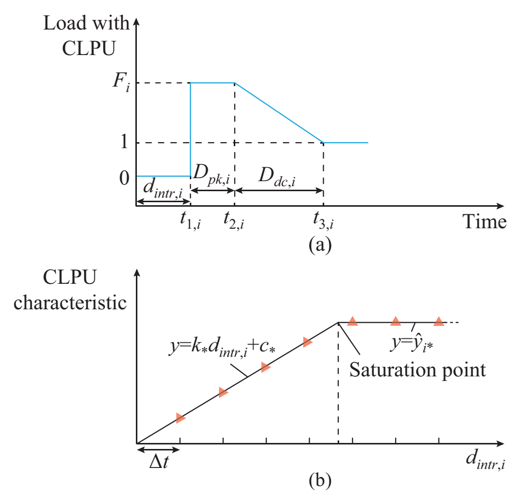

Fig. 2. Modeling of decision-dependent CLPU. (a) Piecewise linear approximation for CLPU curve. (b) Two-stage linear relationship with saturation between CLPU characteristics and CID.

B. Formulation of Linear Constraints

1) Key Characteristics

First, $d_{intr,i}$ is formulated by:

$$d_{intr,i}=\sum_{t\in\mathcal{T}}\left(1-\delta_{i,t}\right)+\alpha_{i,0} \quad \forall i\in\mathcal{N}_X \tag{7}$$

Based on Fig. 2(b), the saturation points of the relationship between CID and the peak magnitude, peak duration, and decay duration of load typ i^* are denoted by $\left(\hat{d}_{F,i*}, \hat{F}_{i*}\right)$, $\left(\hat{d}_{pk,i^*}, \hat{D}_{pk,i^*}\right)$, and $\left(\hat{d}_{dc,i^*}, \hat{D}_{dc,i^*}\right)$, respectively. Accordingly, we derive (8a)-(8c) to represent the relationship between F_i and CID, as depicted by the points marked with triangles.

$$-M\kappa_{F,i} \le d_{intr,i} - \left\lceil \hat{d}_{F,i*} \right\rceil \le M\left(1-\kappa_{F,i}\right) - 1 \quad \forall i \in \mathcal{N}_X \tag{8a}$$

$$-M\left(1-\kappa_{F,i}\right) \le F_i - \left(k_{F,i*} d_{intr,i} + c_{F,i*}\right) \le M\left(1-\kappa_{F,i}\right) \quad \forall i \in \mathcal{N}_X \tag{8b}$$

$$-\hat{F}_{i*}\kappa_{F,i} \le F_i - \hat{F}_{i*} \le 0 \quad \forall i \in \mathcal{N}_X \tag{8c}$$

The relationships for $D_{pk,i}$ and $D_{dc,i}$ can be similarly expressed, which are converted into integers (i.e., multiples of Δt) to facilitate their integration into the discrete-time restoration optimization. The parameter $\varepsilon \in (0,1)$ is introduced to adjust the rounding threshold: round down if the fractional part is below ε, and round up otherwise.

Therefore, we derive (9a)-(9d) to represent the relationship for $D_{pk,i}$, with similar expressions applicable to $D_{dc,i}$.

$$-M\kappa_{pk,i} \le d_{intr,i} - \left\lceil \hat{d}_{pk,i^*} \right\rceil \le M\left(1-\kappa_{pk,i}\right) - 1 \quad \forall i \in \mathcal{N}_X \tag{9a}$$

$$D_{pk,i} - \left(k_{pk,i^*} d_{intr,i} + c_{pk,i^*} + 1 - \varepsilon_{pk}\right) \le M\left(1-\kappa_{pk,i}\right) \quad \forall i \in \mathcal{N}_X \tag{9b}$$

$$-M\left(1-\kappa_{pk,i}\right) \le D_{pk,i} - \left(k_{pk,i^*} d_{intr,i} + c_{pk,i^*} - \varepsilon_{pk}\right) \quad \forall i \in \mathcal{N}_X \tag{9c}$$

$$-M\kappa_{pk,i} \le D_{pk,i} - \left\lceil \hat{D}_{pk,i^*} - \varepsilon_{pk} \right\rceil \le 0 \quad \forall i \in \mathcal{N}_X \tag{9d}$$

2) Decay Rate of CLPU

As a necessary step in load modeling, the decay rate of CLPU is derived as follows, based on the assumption in Fig. 2(a).

$$D_{dc,i} \ne 0 \Rightarrow \Delta f_i D_{dc,i} = F_i - 1 \tag{10}$$

Given that $D_{dc,i}$ is an integer, we can perform the similar binary decomposition, as shown in (4a).

$$D_{dc,i} = \sum_{k=0}^{\left\lfloor \log_2\left\lceil \hat{D}_{dc,i^*} \right\rceil \right\rfloor} 2^k \lambda_{k,i}^{(D)} \quad \forall i \in \mathcal{N}_X \tag{11}$$

Next, a binary variable ξ_i is introduced to indicate the condition when $D_{dc,i} \ne 0$, which can be expressed as $\xi_i = \lambda_{0,i}^{(D)} \vee \lambda_{1,i}^{(D)} \vee \lambda_{2,i}^{(D)} \vee \ldots$ and further formulated by:

$$\xi_i \ge \lambda_{k,i}^{(D)} \quad \forall k \in \mathcal{K}_D, \forall i \in \mathcal{N}_X \tag{12a}$$

$$\xi_i \le \sum_{k=0}^{\left\lfloor \log_2\left\lceil \hat{D}_{dc,i^*} \right\rceil \right\rfloor} \lambda_{k,i}^{(D)} \quad \forall i \in \mathcal{N}_X \tag{12b}$$

Then, similar to (4), the consequent of the logical condition can be expressed by the following linear constraints (13a)-(13c), which impose the correct decay rate.

$$-M\left(1-\lambda_{k,i}^{(D)}\right) \le z_{k,i}^{(\lambda\Delta f)} - \Delta f_i \le 0 \quad \forall k \in \mathcal{K}_D, \forall i \in \mathcal{N}_X \tag{13a}$$

$$0 \le z_{k,i}^{(\lambda\Delta f)} \le M\lambda_{k,i}^{(D)} \quad \forall k \in \mathcal{K}_D, \forall i \in \mathcal{N}_X \tag{13b}$$

$$-M\left(1-\xi_i\right) \le F_i - 1 - \sum_{k=0}^{\left\lfloor \log_2\left\lceil \hat{D}_{dc,i^*} \right\rceil \right\rfloor} 2^k z_{k,i}^{(\lambda\Delta f)} \le M\left(1-\xi_i\right) \quad \forall i \in \mathcal{N}_X \tag{13c}$$

3) Timestamps for Marking Phases

As shown in Fig. 2(a), three timestamps, i.e., $t_{1,i}$, $t_{2,i}$, $t_{3,i}$, divide the restored load into distinct phases: interruption duration, peak duration, decay duration, and steady load of post-CLPU. Consequently, sets of binary variables are introduced to indicate the active phase during any given time span of the restoration process, denoted by:

$$u_{\sim,i,t} = \begin{cases} 0 & t \le t_{\sim,i} \\ 1 & t \ge t_{\sim,i} + 1 \end{cases} \tag{14}$$

Therefore, the above can be enforced by:

$$t_{1,i} = \sum_{t \in \mathcal{T}} \left(1 - \delta_{i,t}\right) \quad \forall i \in \mathcal{N}_X \tag{15a}$$

$$t_{2,i} = t_{1,i} + D_{pk,i} \quad \forall i \in \mathcal{N}_X \tag{15b}$$

$$t_{3,i} = t_{2,i} + D_{dc,i} \quad \forall i \in \mathcal{N}_X \tag{15c}$$

$$-M\left(1-u_{1,i,t}\right) + 1 \le t - t_{1,i} \le M u_{1,i,t} \quad \forall i \in \mathcal{N}_X, \forall t \in \mathcal{T} \tag{15d}$$

$$-M\left(1-u_{2,i,t}\right) + 1 \le t - t_{2,i} \le M u_{2,i,t} \quad \forall i \in \mathcal{N}_X, \forall t \in \mathcal{T} \tag{15e}$$

$$-M\left(1-u_{3,i,t}\right) + 1 \le t - t_{3,i} \le M u_{3,i,t} \quad \forall i \in \mathcal{N}_X, \forall t \in \mathcal{T} \tag{15f}$$

4) Load Representation

We can derive the actual load accounting for CLPU as:

$$P_{L,i,t} = p_{L,i,t} \Big\{ \left(u_{1,i,t} - u_{2,i,t}\right) F_i + \left(u_{2,i,t} - u_{3,i,t}\right) \Big[F_i - \left(t - t_{2,i} - 0.5\right) \Delta f_i \Big] + u_{3,i,t} \Big\} \quad \forall i \in \mathcal{N}_X, \forall t \in \mathcal{T} \tag{16}$$

There are bilinear terms and higher-dimensional products in (16). Nevertheless, most of the involved variables are binary or integer (notably, $u_{1,i,t} - u_{2,i,t}$ and $u_{2,i,t} - u_{3,i,t}$ are binary), facilitating the exact linearization. To achieve this, we introduce auxiliary variables $W_{1,i,t}$, $W_{2,i,t}$, and $W_{3,i,t}$ to substitute for $\left(u_{1,i,t} - u_{2,i,t}\right) F_i$, $\left(u_{2,i,t} - u_{3,i,t}\right) F_i$, and $\left(u_{2,i,t} - u_{3,i,t}\right) \Delta f_i$, respectively, with the following constraints (17a)-(17f) added.

$$-\hat{F}_{i^*}\left(1 - u_{1,i,t} + u_{2,i,t}\right) \le W_{1,i,t} - F_i \le 0 \quad \forall i \in \mathcal{N}_X, \forall t \in \mathcal{T} \tag{17a}$$

$$0 \le W_{1,i,t} \le \hat{F}_{i^*}\left(u_{1,i,t} - u_{2,i,t}\right) \quad \forall i \in \mathcal{N}_X, \forall t \in \mathcal{T} \tag{17b}$$

$$-\hat{F}_{i^*}\left(1 - u_{2,i,t} + u_{3,i,t}\right) \le W_{2,i,t} - F_i \le 0 \quad \forall i \in \mathcal{N}_X, \forall t \in \mathcal{T} \tag{17c}$$

$$0 \le W_{2,i,t} \le \hat{F}_{i^*}\left(u_{2,i,t} - u_{3,i,t}\right) \quad \forall i \in \mathcal{N}_X, \forall t \in \mathcal{T} \tag{17d}$$

$$-M\left(1 - u_{2,i,t} + u_{3,i,t}\right) \le W_{3,i,t} - \Delta f_i \le 0 \quad \forall i \in \mathcal{N}_X, \forall t \in \mathcal{T} \tag{17e}$$

$$0 \le W_{3,i,t} \le M\left(u_{2,i,t} - u_{3,i,t}\right) \quad \forall i \in \mathcal{N}_X, \forall t \in \mathcal{T} \tag{17f}$$

After this, the only remaining bilinear term $t_{2,i} W_{3,i,t}$ can be further linearized using binary decomposition, as $t_{2,i}$ is an integer. With (18a)-(18d), $t_{2,i} W_{3,i,t}$ can be replaced with $W_{4,i,t}$.

$$t_{2,i} = \sum_{k=0}^{\left\lfloor \log_2 \bar{t}_{2,i} \right\rfloor} 2^k \lambda_{k,i}^{(t)} \quad \forall i \in \mathcal{N}_X \tag{18a}$$

$$-M\left(1-\lambda_{k,i}^{(t)}\right) \le z_{k,i,t}^{(\lambda W)} - W_{3,i,t} \le 0 \quad \forall k \in \mathcal{K}_t, \forall i \in \mathcal{N}_X, \forall t \in \mathcal{T} \tag{18b}$$

$$0 \le z_{k,i,t}^{(\lambda W)} \le M\lambda_{k,i}^{(t)} \quad \forall k \in \mathcal{K}_t, \forall i \in \mathcal{N}_X, \forall t \in \mathcal{T} \tag{18c}$$

$$W_{4,i,t} = \sum_{k=0}^{\lfloor \log_2 \bar{t}_{2,i} \rfloor} 2^k z_{k,i,t}^{(\lambda W)} \quad \forall i \in \mathcal{N}_X, \forall t \in \mathcal{T} \tag{18d}$$

Similar to (6), McCormick inequalities can be added, as shown in (19). $\bar{t}_{2,i}$ and $\bar{W}_{3,i,t}$ are the estimated upper bounds for all the possible values of $t_{2,i}$ and $W_{3,i,t}$, respectively.

$$W_{4,i,t} \ge \bar{W}_{3,i,t} t_{2,i} + \bar{t}_{2,i} W_{3,i,t} - \bar{t}_{2,i} \bar{W}_{3,i,t} \quad \forall i \in \mathcal{N}_X, \forall t \in \mathcal{T} \tag{19}$$

Finally, (16) can be rewritten as:

$$P_{L,i,t} = p_{L,i,t}\left[W_{1,i,t} + W_{2,i,t} - (t-0.5)W_{3,i,t} + W_{4,i,t} + u_{3,i,t}\right] \tag{20}$$

Constraint (20) provides a generalized formulation for the interrupted loads throughout the entire restoration horizon. Constraints (17)-(20) collectively replace (16) and are used in the final optimization model to ensure tractability.

IV. Modeling of PDS Restoration Optimization

A. Routing and Scheduling of MESS

As an effective and clean solution for providing emergency supply, MESS is integrated into our restoration process by optimizing its routing and scheduling. The routing model from the authors' previous work [43] is adopted, while the scheduling or operation constraints are expressed by:

$$ch_{j,i,t} + dch_{j,i,t} \le x_{j,i,t} \quad \forall j \in \mathcal{M}, \forall i \in \mathcal{N}_M, \forall t \in \mathcal{T} \tag{21a}$$

$$0 \le P_{c,j,i,t} \le ch_{j,i,t} \cdot P_{c,\max,j} \quad \forall j \in \mathcal{M}, \forall i \in \mathcal{N}_M, \forall t \in \mathcal{T} \tag{21b}$$

$$0 \le P_{d,j,i,t} \le dch_{j,i,t} \cdot P_{d,\max,j} \quad \forall j \in \mathcal{M}, \forall i \in \mathcal{N}_M, \forall t \in \mathcal{T} \tag{21c}$$

$$-x_{j,i,t} Q_{\max,j} \le Q_{j,i,t} \le x_{j,i,t} Q_{\max,j} \quad \forall j \in \mathcal{M}, \forall i \in \mathcal{N}_M, \forall t \in \mathcal{T} \tag{21d}$$

$$\left[\sum_{i \in \mathcal{N}_M}\left(P_{d,j,i,t} - P_{c,j,i,t}\right)\right]^2 + \left(\sum_{i \in \mathcal{N}_M} Q_{j,i,t}\right)^2 \le S_j^2 \quad \forall j \in \mathcal{M}, \forall t \in \mathcal{T} \tag{21e}$$

$$soc_{j,t} = soc_{j,t-1} + \left(e_{c,j}\sum_{i \in \mathcal{N}_M} P_{c,j,i,t} - \frac{\sum_{i \in \mathcal{N}_M} P_{d,j,i,t}}{e_{d,j}}\right)\frac{\Delta t}{E_j} \quad \forall j \in \mathcal{M}, \forall t \in \mathcal{T} \tag{21f}$$

$$soc_{j,\min} \le soc_{j,t} \le soc_{j,\max} \quad \forall j \in \mathcal{M}, \forall t \in \mathcal{T} \tag{21g}$$

B. Network Reconfiguration

The flow-based model from [44] is used to formulate the network reconfiguration of PDS, facilitating the formation of microgrids to supply interrupted loads as follows. Note that i_r represents the substation node.

$$\sum_{(i',i_r) \in \mathcal{L}} f_{i'i_r,t}^{i_x} - \sum_{(i_r,i') \in \mathcal{L}} f_{i_r i',t}^{i_x} = -1 \quad \forall t \in \mathcal{T}, \forall i_x \in \mathcal{N} \backslash i_r \tag{22a}$$

$$\sum_{(i',i_x) \in \mathcal{L}} f_{i'i_x,t}^{i_x} - \sum_{(i_x,i') \in \mathcal{L}} f_{i_x i',t}^{i_x} = 1 \quad \forall t \in \mathcal{T}, \forall i_x \in \mathcal{N} \backslash i_r \tag{22b}$$

$$\sum_{(i',i) \in \mathcal{L}} f_{i'i,t}^{i_x} - \sum_{(i,i') \in \mathcal{L}} f_{ii',t}^{i_x} = 0 \quad \forall t \in \mathcal{T}, \forall i_x \in \mathcal{N} \backslash i_r, \forall i \in \mathcal{N} \backslash \left\{i_x, i_r\right\} \tag{22c}$$

$$\begin{cases} 0 \le f_{i'i,t}^{i_x} \le \lambda_{i'i,t} \\ 0 \le f_{ii',t}^{i_x} \le \lambda_{ii',t} \end{cases} \quad \forall t \in \mathcal{T}, \forall i_x \in \mathcal{N} \backslash i_r, \forall (i',i) \in \mathcal{L} \tag{22d}$$

$$\sum_{(i',i) \in \mathcal{L}} \left(\lambda_{i'i,t} + \lambda_{ii',t}\right) = |\mathcal{N}| - 1 \quad \forall t \in \mathcal{T} \tag{22e}$$

$$\lambda_{i'i,t} + \lambda_{ii',t} = \mu_{i'i,t} \quad \forall t \in \mathcal{T}, \forall (i',i) \in \mathcal{L} \tag{22f}$$

$$\upsilon_{i'i,t} \le \mu_{i'i,t} \quad \forall t \in \mathcal{T}, \forall (i',i) \in \mathcal{L} \tag{22g}$$

$$\upsilon_{i'i,t} = 0 \quad \forall (i',i) \in \mathcal{L}_{out,t} \tag{22h}$$

C. PDS Operation

The widely-used linearized DistFlow model is adopted as operation constraints of the PDS [4], [6], incorporating backup distributed generators. Specifically, $P_{L,i,t}$ is used in the power balance constraints, thereby embedding the CLPU effect into the operation and restoration process. $[\![\cdot]\!]$ denotes the Iverson bracket, which equals 1 if the condition is true and 0 otherwise.

$$P_{IN,i,t} = [\![i \in \mathcal{N}_M]\!] \sum_{j \in \mathcal{M}} \left(P_{d,j,i,t} - P_{c,j,i,t}\right) + P_{DG,i,t} \quad \forall t \in \mathcal{T}, \forall i \in \mathcal{N} \tag{23a}$$

$$Q_{IN,i,t} = [\![i \in \mathcal{N}_M]\!] \sum_{j \in \mathcal{M}} Q_{j,i,t} + Q_{DG,i,t} \quad \forall t \in \mathcal{T}, \forall i \in \mathcal{N} \tag{23b}$$

$$\sum_{(i',i) \in \mathcal{L}} P_{i'i,t} + P_{IN,i,t} - P_{L,i,t} = \sum_{(i,i') \in \mathcal{L}} P_{ii',t} \quad \forall t \in \mathcal{T}, \forall i \in \mathcal{N} \tag{23c}$$

$$\sum_{(i',i) \in \mathcal{L}} Q_{i'i,t} + Q_{IN,i,t} - Q_{L,i,t} = \sum_{(i,i') \in \mathcal{L}} Q_{ii',t} \quad \forall t \in \mathcal{T}, \forall i \in \mathcal{N} \tag{23d}$$

$$Q_{L,i,t} = \eta_i P_{L,i,t} \quad \forall t \in \mathcal{T}, \forall i \in \mathcal{N}_X \tag{23e}$$

$$\begin{cases} V_{i,t}^2 \ge V_{i',t}^2 - 2\left(P_{i'i,t} r_{i'i} + Q_{i'i,t} x_{i'i}\right) - M\left(1-\upsilon_{i'i,t}\right) \\ V_{i,t}^2 \le V_{i',t}^2 - 2\left(P_{i'i,t} r_{i'i} + Q_{i'i,t} x_{i'i}\right) + M\left(1-\upsilon_{i'i,t}\right) \end{cases} \quad \forall t \in \mathcal{T}, \forall (i',i) \in \mathcal{L} \tag{23f}$$

$$V_{i,\min}^2 \le V_{i,t}^2 \le V_{i,\max}^2 \quad \forall t \in \mathcal{T}, \forall i \in \mathcal{N} \tag{23g}$$

$$P_{i'i,t}^2 + Q_{i'i,t}^2 \le \upsilon_{i'i,t} S_{i'i}^2 \quad \forall t \in \mathcal{T}, \forall (i',i) \in \mathcal{L} \tag{23h}$$

$$\delta_{i,t} \ge \delta_{i,t-1} \quad \forall t \in \mathcal{T}, \forall i \in \mathcal{N}_X \tag{23i}$$

$$P_{DG,i,t}^2 + Q_{DG,i,t}^2 \le S_{DG,i}^2 \quad \forall t \in \mathcal{T}, \forall i \in \mathcal{N} \tag{23j}$$

D. Objective Function for Restoration

The proposed approach aims to restore the interrupted loads with the objective of minimizing the total CIC, as represented by the first term in (24). In addition, costs associated with deploying MESS, operating distributed generators, and switching branches are included to avoid futile MESS movements, generator operations, and switching actions. The objective function is thus formulated as:

$$\min \left\{\sum_{t \in \mathcal{T}} \sum_{i \in \mathcal{N}_X} p_{L,i,t} A_{i,t}^{fun} \Delta t + \sigma_1 \sum_{t \in \mathcal{T}} \sum_{m \in \mathcal{M}} \sum_{i \in \mathcal{N}_M} v_{j,i,t} + \sigma_2 \sum_{t \in \mathcal{T}} \sum_{i \in \mathcal{N}} P_{DG,i,t} + \sigma_3 \sum_{t \in \mathcal{T}} \sum_{(i',i) \in \mathcal{L}} \left|\upsilon_{i'i,t} - \upsilon_{i'i,t-1}\right|\right\} \tag{24}$$

Given that $\left|v_{i'i,t}-v_{i'i,t-1}\right|$ can be equally written as $\max\left\{v_{i'i,t}-v_{i'i,t-1}, v_{i'i,t-1}-v_{i'i,t}\right\}$, we introduce an auxiliary variable $\Delta v_{i'i,t}$ to replace $|v_{i'i,t}-v_{i'i,t-1}|$ with the following constraints imposed, thereby converting (24) into a linear form.

$$\begin{cases} \Delta v_{i'i,t} \geq v_{i'i,t}-v_{i'i,t-1} \\ \Delta v_{i'i,t} \geq v_{i'i,t-1}-v_{i'i,t} \end{cases} \tag{25}$$

Moreover, while $P_{L,i,t}$ does not appear explicitly in (24), it affects the restoration outcome through (23), which governs the feasibility of load restoration. In this way, the CLPU model indirectly but decisively influences CIDs, hence the total CIC is minimized.

V. Case Studies

Case studies are conducted to validate the effectiveness of the proposed approach. While (21e), (23h), and (23j) can be linearized using the approach from [45], the mixed-integer linear programming (MILP) model for PDS restoration optimization is programmed in MATLAB using the YALMIP toolbox [46] and solved by Gurobi v11.0.0.

A. Benchmark Test on IEEE 33-node System

1) System Setup

IEEE 33-node system is used for test and illustrated in Fig. 3, with detailed parameters available in [47] and the dashed lines denote normally open tie lines. We set up initial damages on 7 branches to construct the testing scenario. Since this study focuses on modeling CIC and CID rather than detailing a resource-intensive PDS restoration, the repairs for these damaged branches are assumed predefined and occur in two stages, as shown in Table I. The scheduling horizon is set to be 9 hours, with each time span representing 30 min.

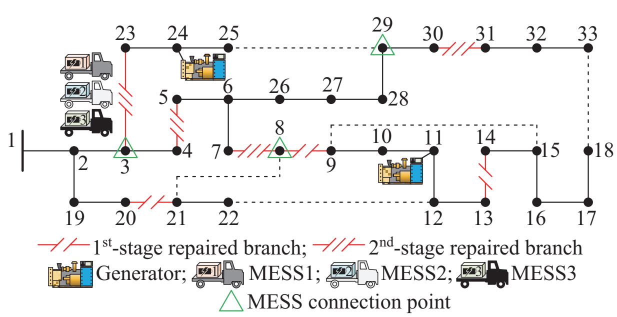

Fig. 3. IEEE 33-node system.

TABLE I
DAMAGED BRANCHES IN IEEE 33-NODE SYSTEM

Stage	Sets of damaged branches
Stage 1: 1st to 7th time spans	(20, 21), (8, 9), (13, 14), (3, 23), (4, 5), (7, 8), (30, 31)
Stage 2: 8th to 11th time spans	(3, 23), (4, 5), (7, 8), (30, 31)

The loads are arbitrarily divided into residential and CI types, with variations in their CIC relative to CID that is modeled according to the parameters in Fig. 1. The initial CID $\alpha_{i,0}$ is uniformly set to be 1, corresponding to an initial interruption of 30 min, except for the nodes continuously connected to the substation node 1. The relationships between CLPU characteristics and CID, as shown in Fig. 4, are assumed for CLPU modeling. In practice, these relationships can be derived from simulated or historical CLPU data in various CID scenarios. However, as this lies outside the scope of this study, we make a direct assumption here. Details on relevant simulation methodologies can be found in [33]-[35] and [48].

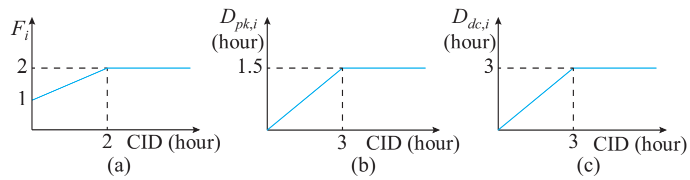

Fig. 4. Relationships between CLPU characteristics and CID. (a) F_i. (b) $D_{pk,i}$. (c) $D_{dc,i}$.

Three 500 kW/1000 kWh MESS units are dispatched during the restoration process. Three MESS connection points are assumed at nodes 3, 8, and 29 within the PDS. The travel time between nodes 3 and 29 is set to be 2 time spans, while for other node pairs, it is set to be 1 time span. The MESS units are initially located at node 3 with an initial state of charge of 0.9 p.u.. In addition, two 800 kW/1000 kVA generators are available at nodes 11 and 24.

2) Result Analysis

The main results are presented as follows. First, we examine the overall restoration process, and the results are shown in Fig. 5. The PDS is initially reconfigured into two islands, which are subsequently reconnected to the main grid as the damaged branches are gradually repaired after the 7th and 11th time spans. During this process, the network reconfiguration requires only two necessary steps: closing branch 20-21 after the 7th time span and closing branch 3-23 after the 11th time span. Other damaged branches, even after repair, do not need further operation to maintain the radial structure of the PDS and minimize the switching actions, as dedicated by the last term of the objective function (24).

The three MESSs are deployed to the two islands at the start of the restoration process, as shown in Figs. 5 and 6. Notably, MESS1 departs from island 2 before it reconnects to the main grid. This is because the CLPU process of the restored loads within island 2 has already subsided. The load has dropped to a level that the generator at node 11 can sustain by itself, giving MESS1 the opportunity to leave and supply another island. Then, as load 11 is restored during the 7th time span, the generator alone would be insufficient to sustain island 2. Consequently, MESS3 arrives to provide supplementary power. Once island 2 reconnects to the grid, MESS3 and MESS2, which have just arrived due to proximity to node 8, charge and then return to island 1 to supply power.

Specifically, Fig. 7(a) and (b) presents the results of $A_{i,t}^{fun}$ under different initial CIDs, with the current case referred to as the benchmark case. For clearer demonstration, we also provide the results for two additional cases with increased initial CIDs, as shown in Fig. 7(c)-(f). Nodes 23 and 30 are selected to represent the two customer types, i.e., residential and CI customers, respectively. For clarity, the y-axis ranges are unified within each type to ensure a fair visual comparison of CIC variations with respect to CID. These results indicate that the proposed approach effectively reproduces the relationship between CIC and CID shown in Fig. 1. In addition, as shown by the shaded area in Fig. 7(f), the proposed approach ensures a rational and monotonic CIC behavior by properly handling the crossing point in the quadratic formulation, as enforced by constraint (3c). Specifically, once the quadratic function drops below zero, the CIC rate is assigned a small positive constant, indicating that CIC continues to increase but at a very slow rate. These results confirm that the proposed approach is precise and objective for quantifying CIC and formulating objectives in restoration optimization modeling.

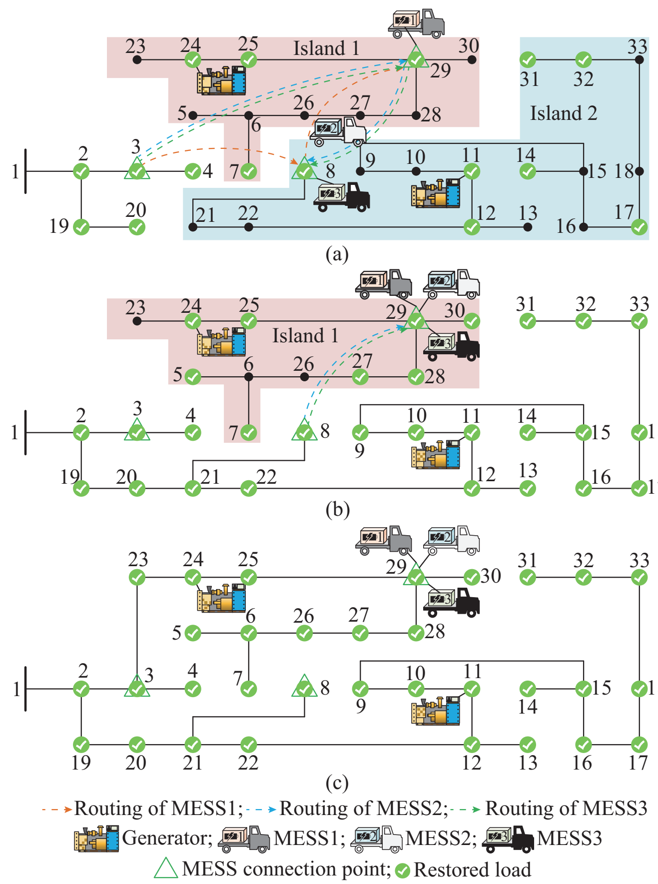

Fig. 5. Results of restoration process. (a) 1st to 7th time spans. (b) 8th to 11th time spans. (c) 12th to 18th time spans.

Figure 8 presents the results of load states, where the flag symbol denotes the CI customers, emphasizing on the distribution of different phases in the post-restoration CLPU process for all loads, revealing the anticipated variations in CLPU timing characteristics across different CID conditions. To further highlight our findings, we showcase several typical restored load curves in Fig. 9 to more clearly illustrate the variations in CLPU, where the loads have been normalized by their original values without CLPU. As CID gradually increases, the peak magnitude, peak duration, and decay duration all increase correspondingly. Once CID exceeds the respective saturation points, these characteristics stabilize at their maximum values. As demonstrated, the proposed approach effectively captures and reproduces the predefined relationships between CLPU and CID shown in Fig. 4, enabling dynamic representation of CLPU relative to CID and enhancing the modeling precision of load restoration behavior. This, in turn, facilitates efficient emergency resource deployment and more effective restoration strategies. Notably, without such dynamic representation, CLPU may be overestimated or underestimated during certain periods, leading to excessive deployment of unnecessary resources or rendering optimal decisions practically infeasible.

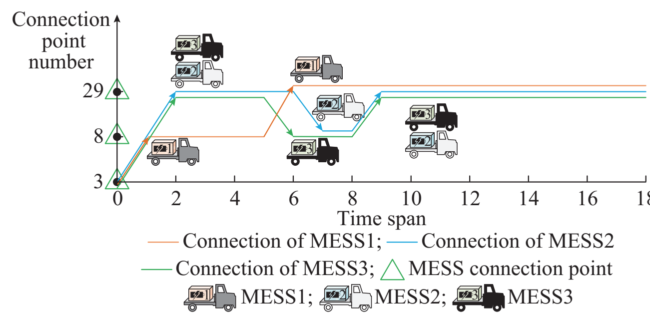

Fig. 6. Routing results of MESSs.

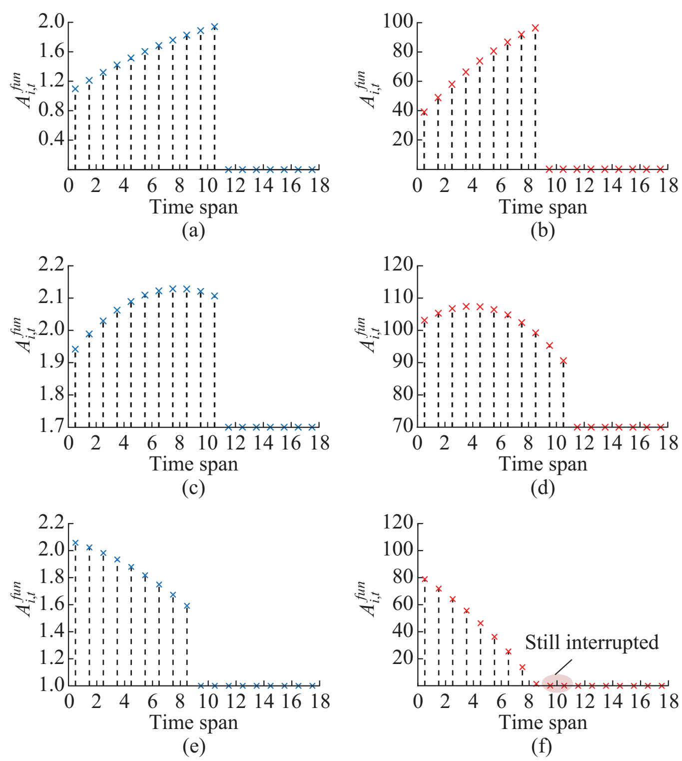

Fig. 7. Results of $A_{i,t}^{fun}$ under different initial CIDs. (a) Node 23 under benchmark case. (b) Node 30 under benchmark case. (c) Node 23 under a case with an initial CID of 5.5 hours. (d) Node 30 under a case with an initial CID of 5.5 hours. (e) Node 23 under a case with an initial CID of 11.5 hours. (f) Node 30 under a case with an initial CID of 11.5 hours.

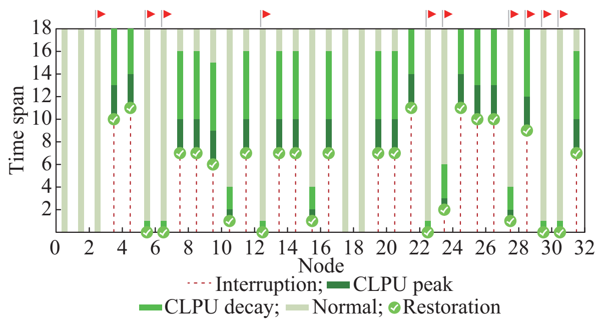

Fig. 8. Results of load states.

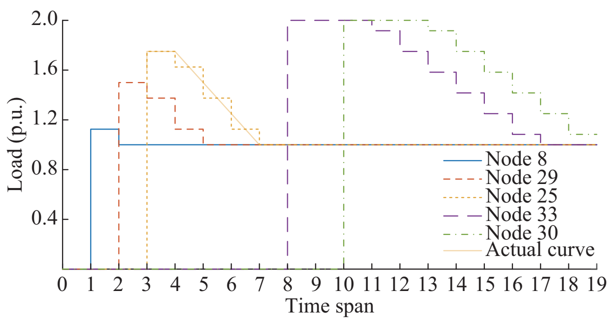

Fig. 9. Typical restored load curves incorporating decision-dependent CLPU.

3) Dynamic Rating by MESS

To further reveal the potential of MESS in enhancing restoration performance, particularly under the influence of CLPU, we present the power demand and supply results for the two islands, as illustrated in Fig. 10(a) under the benchmark case. Since the two islands reconnect to the main grid after the 7th time span and 11th time span, respectively, only the profiles before these periods are plotted.

For comparison, we also simulate two additional cases as follows. The corresponding results are presented in Fig. 10(c), (d) and Fig. 10(e), (f), respectively.

1) Case 1: with stationary MESSs that are fixed at their initial locations within the islands

2) Case 2: with all MESSs omitted.

It can be observed that the generators serve as the primary power supply, nearly operating at the maximum capacity at all times to support the restored loads. However, the CLPU following load restoration often drives power demand beyond the generator capability. In such situations, MESS provides short-term support to address this excessive power demand. Once the CLPU subsides and the power demand falls back within the generator capacity, the MESS can leave, as clearly demonstrated by the behavior of MESS1 in island 2.

This observation underscores the pivotal role of MESS as a service provider of dynamic rating during the PDS restoration process, and this term originally coined in the context of transmission lines to describe the temporary boost in transmission capacity to deliver more power when needed. Similarly, during restoration, MESS temporarily augments the total supply capacity of isolated islands, enabling them to withstand temporary load surges, such as those induced by CLPU. Without such temporary support, the restored loads would have to be reduced to limit the load surges. Furthermore, the mobility of MESS facilitates the flexibility of dynamic rating service. Once the CLPU-induced load surges subside, the additional capacity provided by MESS can be released, allowing the MESS to relocate to other islands and continue supporting their restoration efforts. For a more intuitive comparison, the total CICs for the benchmark case, and cases 1 and 2 are \$91526, \$134760, and \$271340, respectively. This indicates that the utilization of MESS reduces the total CICs by 32% and 66%, respectively, compared with those in cases 1 and 2.

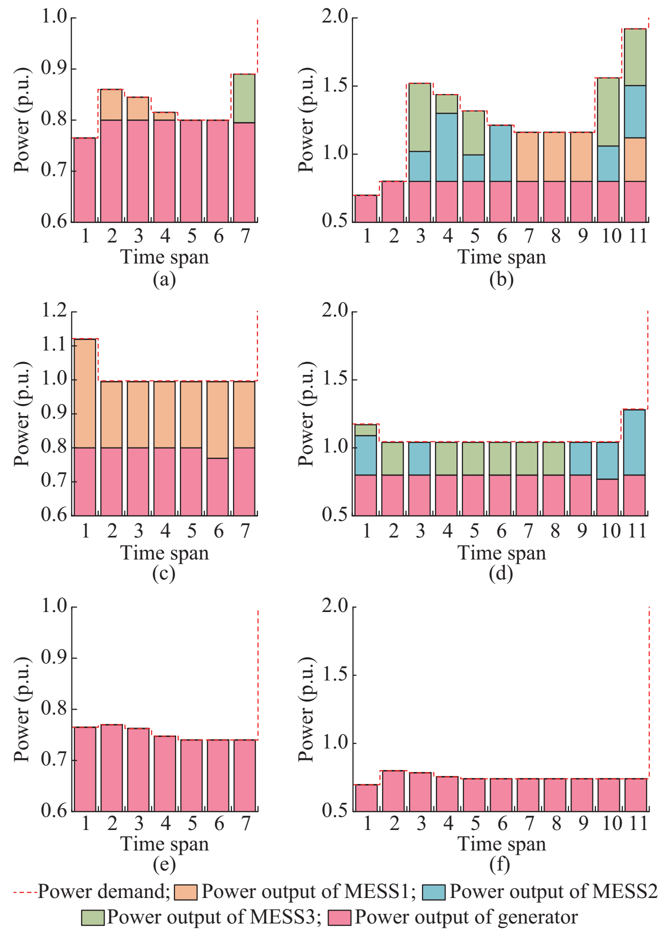

Fig. 10. Results of power demand and power outputs of MESS and generator of island 2 and island 1 under different cases. (a) Benchmark case with island 2. (b) Benchmark case with island 1. (c) Case 1 with island 2. (d) Case 1 with island 1. (e) Case 2 with island 2. (f) Case 2 with island 1.

B. Sensitivity Analysis

We further conduct sensitivity analyses on certain key parameters including CIC modeling, CLPU characteristic, and initial CID. These analyses aim to further validate the effectiveness of the proposed approach and reveal how restoration processes evolve in varying scenarios.

1) CIC Modeling

In the decision-dependent CIC model, the increasing rate of CIC varies quadratically with CID. In this part, the decision-dependent CIC model is compared against the conventional constant-rate model, which assumes a fixed CIC per unit time, i.e., the quadratic coefficients are set to be zero except c_{i^*}. To enable a clearer comparison, we modify the scenario setup for the IEEE 33-node system. As illustrated in Supplementary Material A Fig. SA1(a), we assume seven branch damages and slightly adjust a few loads to split the system into two islands with equal total loads, where all loads are set as residential, thereby enabling a more neutral comparison of the restoration paths. All damaged branches are repaired by the end of the 12^{th} time span. In addition, the initial CID is set to be 3 hours for all loads in island 1 and 9 hours in island 2, to better illustrate how CIC variation shapes restoration paths. Both values are set above 3 hours to ensure full saturation of CLPU characteristics across all loads, thereby isolating their influence from the CIC-driven restoration.

The comparative results under the proposed decision-dependent CIC model and conventional constant-rate model are shown in Supplementary Material A Fig. SA1. The comparison highlights that the proposed decision-dependent CIC model enables restoration decisions to better align with dynamic economic priorities, which is more nuanced and responsive.

2) CLPU Characteristics

To assess the sensitivity of the CLPU model, we examine the impact of key CLPU characteristics on restoration outcomes. Specifically, based on the benchmark case, we vary the maximum peak magnitude, the maximum peak duration, and the maximum decay duration (all referring to their saturated values). Results in Supplementary Material A Fig. SA2 confirm that total CIC increases with higher peak magnitude and longer decay duration, highlighting the importance of incorporating CLPU temporal dynamics into restoration modeling.

3) Initial CID

Further sensitivity analysis is conducted by varying the initial CID to evaluate its impact on restoration performance. Specifically, 12 test cases are implemented with initial CID ranging from 0.5 hours to 6 hours in the increment of 0.5 hours. Results in Supplementary Material A Fig. SA3 validate the capability of the proposed approach to capture the relationship between CLPU characteristics and CID, as well as its significance in restoration optimization.

C. Scalability Test and Discussion

To further evaluate the scalability of the proposed approach, additional simulation is carried out on a modified IEEE 123-node system [49]. The test system, results, and the discussion on the computation burden are provided in Supplementary Material B.

VI. Conclusion

Incorporating the decision-dependencies of CIC and CLPU into PDS restoration decision-making is critical for developing effective and practical restoration strategies. However, modeling these dependencies is challenging due to the limited understanding of the underlying physical mechanisms. Inspired by the principles of data-driven optimization, this study proposes a tractable modeling approach for decision-dependent CIC and CLPU for optimizing PDS restoration, captures and represents their variations with CID based on data-derived patterns rather than explicit physical modeling. All related constraints are formulated in linear forms, enabling the subsequent construction of a comprehensive and tractable PDS restoration optimization model that integrates MESS scheduling and network reconfiguration. Extensive case studies verify the effectiveness of the proposed approach and highlight the role of MESS in providing a temporary dynamic rating service, thereby enhancing restoration performance under CLPU conditions.

This study serves as a stepping stone toward addressing the decision-dependencies of CIC and CLPU for optimizing PDS restoration. It is worth mentioning that, although the proposed approach relies on data-driven surrogate models for CIC and CLPU, its robustness to moderate data variability is supported by several factors. First, the surrogate functions are obtained via data fitting with shape constraints, which inherently mitigate the influence of noise and outliers while preserving realistic trends. Second, the sensitivity analyses indicate that variations in key parameters lead primarily to quantitative adjustments in the optimal restoration decisions while leaving the overall strategy intact. In practice, the surrogates can be re-trained with updated measurements, ensuring adaptability in evolving system conditions, and future work will explore robust or uncertainty-aware models to further enhance reliability under data uncertainty.

Looking ahead, future research will also focus on two complementary directions: developing fully analytical models grounded in a deeper investigation of the underlying physical mechanisms behind these decision-dependencies to improve interpretability, or refining the data-driven surrogate modeling techniques to achieve higher fidelity and computational efficiency within an optimization framework. These efforts will further enhance the practicality and robustness of the decision-dependent PDS restoration strategies.

References

[1] S. A. Arefifar, M. S. Alam, and A. Hamadi, "A review on self-healing in modern power distribution systems," *Journal of Modern Power Systems and Clean Energy*, vol. 11, no. 6, pp. 1719-1733, Nov. 2023.

[2] Y. Wang, Y. Xue, D. Xie *et al.*, "Stochastic optimization of medium- and short-term reserve arrangement for preventive and emergency control under typhoon disaster," *Journal of Modern Power Systems and Clean Energy*, vol. 13, no. 1, pp. 190-201, Jan. 2025.

[3] B. V. Venkatasubramanian and M. Panteli, "Power system resilience during 2001–2022: a bibliometric and correlation analysis," *Renewable and Sustainable Energy Reviews*, vol. 188, p. 113862, Dec. 2023.

[4] C. Chen, J. Wang, F. Qiu *et al.*, "Resilient distribution system by microgrids formation after natural disasters," *IEEE Transactions on Smart Grid*, vol. 7, no. 2, pp. 958-966, Mar. 2016.

[5] L. Yan, M. Sheikholeslami, W. Gong *et al.*, "Architecture, control, and implementation of networked microgrids for future distribution systems," *Journal of Modern Power Systems and Clean Energy*, vol. 10, no. 2, pp. 286-299, Mar. 2022.

[6] S. Lei, C. Chen, H. Zhou *et al.*, "Routing and scheduling of mobile power sources for distribution system resilience enhancement," *IEEE Transactions on Smart Grid*, vol. 10, no. 5, pp. 5650-5662, Sept. 2019.

[7] W. Wang, X. Xiong, Y. He *et al.*, "Scheduling of separable mobile energy storage systems with mobile generators and fuel tankers to boost distribution system resilience," *IEEE Transactions on Smart Grid*, vol. 13, no. 1, pp. 443-457, Jan. 2022.

[8] G. Song, C. Ma, H. Ji *et al.*, "Bi-level supply restoration method for active distribution networks considering multi-resource coordination," *Journal of Modern Power Systems and Clean Energy*, vol. 13, no. 3, pp. 967-979, May 2024.

[9] B. Li, Y. Chen, W. Wei *et al*., “Resilient restoration of distribution systems in coordination with electric bus scheduling,” *IEEE Transactions on Smart Grid*, vol. 12, no. 4, pp. 3314-3325, Jul. 2021.
[10] S. Badakhshan, J. Rahman, and J. Zhang, “Black start of coastline power networks from grid-forming ship-to-grid services,” *IEEE Transactions on Smart Grid*, vol. 15, no. 2, pp. 1670-1679, Mar. 2024.
[11] S. Yao, P. Wang, X. Liu *et al*., “Rolling optimization of mobile energy storage fleets for resilient service restoration,” *IEEE Transactions on Smart Grid*, vol. 11, no. 2, pp. 1030-1043, Mar. 2020.
[12] Y. Li, W. Sun, W. Yin *et al*., “Restoration strategy for active distribution systems considering endogenous uncertainty in cold load pickup,” *IEEE Transactions on Smart Grid*, vol. 13, no. 4, pp. 2690-2702, Jul. 2022.
[13] R. Billinton and P. Wang, “Distribution system reliability cost/worth analysis using analytical and sequential simulation techniques,” *IEEE Transactions on Power Systems*, vol. 13, no. 4, pp. 1245-1250, Nov. 1998.
[14] G. H. KjØlle, K. Samdal, B. Singh *et al*., “Customer costs related to interruptions and voltage problems: methodology and results,” *IEEE Transactions on Power Systems*, vol. 23, no. 3, pp. 1030-1038, Aug. 2008.
[15] Ernest Orlando Lawrence Berkeley National Laboratory. (2015, Jan.). Updated value of service reliability estimates for electric utility customers in the United States. [Online]. Available: https://emp. lbl. gov/publications/updated-value-service-reliability
[16] Ernest Orlando Lawrence Berkeley National Laboratory. (2018, Jul.). Estimating power system interruption costs: a guidebook for electric utilities. [Online]. Available: https://emp.lbl.gov/publications/estimating-power-system-interruption
[17] International Energy Agency. (2018, May). The future of cooling: opportunities for energy-efficient air conditioning. [Online]. Available: https://www.iea.org/reports/the-future-of-cooling
[18] J. Hong and D. Montero. (2024, Aug.). Keeping cool on a hotter planet. [Online]. Available: https://www. chinadaily. com. cn/a/202304/24/WS6445cd7ca310b6054facf517.html
[19] The IEEE Power Engineering Society. (2004, Jan.). Working group D1: cold load pickup issues. [Online]. Available: https://www.pes-psrc.org/kb/report/075.pdf
[20] B. Chen, C. Chen, J. Wang *et al*., “Multi-time step service restoration for advanced distribution systems and microgrids,” *IEEE Transactions on Smart Grid*, vol. 9, no. 6, pp. 6793-6805, Nov. 2018.
[21] C Hachmann, G Lammert, L Hamann *et al*., “Cold load pickup model parameters based on measurements in distribution systems,” *IET Generation, Transmission, and Distribution*, vol. 13, no. 23, pp. 5387-5395, Nov. 2019.
[22] Austin Energy. (2025, Jul.). Winter power outage update – Feb. 2, 2023, 4 p.m. [Online]. Available: https://austinenergy.com/about/news/news-releases/2023/winter-power-outage-update-feb-2-2023-4-pm
[23] S. Ihara and F. C. Schweppe, “Physically based modeling of cold load pickup,” *IEEE Transactions on Power Apparatus and Systems*, vol. PAS-100, no. 9, pp. 4142-4150, Sept. 1981.
[24] R. Fan, R. Sun, Y. Liu *et al*., “Adaptive power load restoration considering flexible control of air conditioners for resilience enhancement,” *International Journal of Electrical Power & Energy Systems*, vol. 148, p. 108959, Jun. 2023.
[25] Q. Meng, T. Gao, X. Zhang *et al*., “Load rebound suppression strategy and demand response potential of thermal storage HVAC systems: an experimental and simulation study,” *Journal of Energy Storage*, vol. 73, p. 108872, Dec. 2023.
[26] W. Wang, Y. He, X. Xiong *et al*., “Robust survivability-oriented scheduling of separable mobile energy storage and demand response for isolated distribution systems,” *IEEE Transactions on Power Delivery*, vol. 37, no. 5, pp. 3521-3535, Oct. 2022.
[27] E. A. M. Ceseña, N. Good, and P. Mancarella, “Electrical network capacity support from demand side response: techno-economic assessment of potential business cases for small commercial and residential end-users,” *Energy Policy*, vol. 82, pp. 222-232, Jul. 2015.
[28] R. Hu, A. Shirsat, V. Muthukaruppan *et al*., “Adaptive cold-load pickup considerations in 2-stage microgrid unit commitment for enhancing microgrid resilience,” *Applied Energy*, vol. 356, p. 122424, Feb. 2024.
[29] J. Zheng, G. Laparra, G. Zhu *et al*., “Aggregate power control of heterogeneous TCL populations governed by Fokker–Planck equations,” *IEEE Transactions on Control Systems Technology*, vol. 28, no. 5, pp. 1915-1927, Sept. 2020.
[30] M. Song, R. R. Nejad, and W. Sun, “Robust distribution system load restoration with time-dependent cold load pickup,” *IEEE Transactions on Power Systems*, vol. 36, no. 4, pp. 3204-3215, Jul. 2021.
[31] Y. Li, W. Sun, W. Yin *et al*., “Restoration strategy for active distribution systems considering endogenous uncertainty in cold load pickup,” *IEEE Transactions on Smart Grid*, vol. 13, no. 4, pp. 2690-2702, Jul. 2022.
[32] Y. Wang, X. Su, M. Song *et al*., “Sequential load restoration with soft open points and time-dependent cold load pickup for resilient distribution systems,” *IEEE Transactions on Smart Grid*, vol. 14, no. 5, pp. 3427-3438, Sept. 2023.
[33] Z. Zhai and Q. Chen, “Performance of coupled building energy and CFD simulations,” *Energy and Buildings*, vol. 37, no. 4, pp. 333-344, Apr. 2005.
[34] M. Rajput, G. Augenbroe, B. Stone *et al*., “Heat exposure during a power outage: a simulation study of residences across the Metro Phoenix area,” *Energy and Buildings*, vol. 259, p. 111605, Mar. 2022.
[35] T. Hoyt, E. Arens, and H. Zhang, “Extending air temperature setpoints: simulated energy savings and design considerations for new and retrofit buildings,” *Building and Environment*, vol. 88, pp. 89-96, Jun. 2015.
[36] Y. Jin, H. Wang, T. Chugh *et al*., “Data-driven evolutionary optimization: an overview and case studies,” *IEEE Transactions on Evolutionary Computation*, vol. 23, no. 3, pp. 442-458, Jun. 2019.
[37] L. Hong and X. Zhang, “Surrogate-based simulation optimization,” *INFORMS Tutorials in Operations Research*, vol. 10, pp. 287-311, Oct. 2021.
[38] G. Wang and S. Shan, “Review of metamodeling techniques in support of engineering design optimization,” *ASME Journal of Mechanical Design*, vol. 129, no. 4, pp. 370-380, Apr. 2007.
[39] X. Wan, J. F. Pekny, and G. V. Reklaitis, “Simulation-based optimization with surrogate models–application to supply chain management,” *Computers & Chemical Engineering*, vol. 29, no. 6, pp. 1317-1328, May 2005.
[40] G. Wacker, E. Wojczynski, and R. Billinton, “Interruption cost methodology and results–a Canadian residential survey,” *IEEE Transactions on Power Apparatus and Systems*, vol. PAS-102, no. 10, pp. 3385-3392, Oct. 1983.
[41] A Billionnet, S Elloumi, and A Lambert, “Exact quadratic convex reformulations of mixed-integer quadratically constrained problems,” *Mathematical Programming*, vol. 158, pp. 235-266, Jul. 2016.
[42] S. Liu, C. Chen, Y. Jiang *et al*., “Bi-level coordinated power system restoration model considering the support of multiple flexible resources,” *IEEE Transactions on Power Systems*, vol. 38, no. 2, pp. 1583-1595, Mar. 2023.
[43] W. Wang, X. Xiong, C. Xiao *et al*., “A novel mobility model to support the routing of mobile energy resources,” *IEEE Transactions on Smart Grid*, vol. 13, no. 4, pp. 2675-2678, Jul. 2022.
[44] S. Lei, C. Chen, Y. Song *et al*., “Radiality constraints for resilient reconfiguration of distribution systems: formulation and application to microgrid formation,” *IEEE Transactions on Smart Grid*, vol. 11, no. 5, pp. 3944-3956, Sept. 2020.
[45] X. Chen, W. Wu, and B. Zhang, “Robust restoration method for active distribution networks,” *IEEE Transactions on Power Systems*, vol. 31, no. 5, pp. 4005-4015, Sept. 2016.
[46] J. Löfberg, “YALMIP: a toolbox for modeling and optimization in MATLAB,” in *Proceedings of 2004 IEEE International Symposium on Computer Aided Control Systems Design*, Taibei, China, Sept. 2004, pp. 284-289.
[47] M. E. Baran and F. F. Wu, “Network reconfiguration in distribution systems for loss reduction and load balancing,” *IEEE Transactions on Power Delivery*, vol. 4, no. 2, pp. 1401-1407, Apr. 1989.
[48] K. P. Schneider, E. Sortomme, S. S. Venkata *et al*., “Evaluating the magnitude and duration of cold load pick-up on residential distribution using multi-state load models,” *IEEE Transactions on Power Systems*, vol. 31, no. 5, pp. 3765-3774, Sept. 2016.
[49] IEEE. (2024, Jan.). IEEE PES test feeder. [Online]. Available: https://cmte.ieee.org/pes-testfeeders/resources/

Wei Wang received the B.E. degree in electrical engineering from Southwest Jiaotong University, Chengdu, China, in 2014, and the M.E. and Ph.D. degrees in electrical engineering from Chongqing University, Chongqing, China, in 2017 and 2021, respectively. He is currently an Assistant Professor with Southwest Jiaotong University. His research interests include power and energy system resilience, restoration, and emergency resource scheduling.

Minwu Chen received the B.E. and Ph.D. degrees in electrical engineering from Southwest Jiaotong University, Chengdu, China, in 2004 and 2009, respectively. He is currently a Full Professor with Southwest Jiaotong University. His research interests include energy management and secure operation of power and transportation systems.

Hongbin Wang received the M.E. and Ph.D. degrees in electrical engineering from Chongqing University, Chongqing, China, in 2012 and 2025, respectively. He is a Senior Engineer with the Electric Power Research Institute of State Grid Chongqing Electric Power Company, Chongqing, China. His research interests include power system protection and restoration.

Gaoqiang Peng received the M.E. degree from Southwest Petroleum University, Chengdu, China, in 2021. He is currently pursuing the Ph.D. degree in electrical engineering with the School of Electrical Engineering, Southwest Jiaotong University, Chengdu, China. His research interests include power system resilience and energy management.

Hongzhou Chen received the B.E. degree in electrical engineering from the China University of Petroleum, Qingdao, China, in 2019, and the Ph.D. degree in electrical engineering from Chongqing University, Chongqing, China, in 2024. He is currently a Postdoctoral Researcher with the Electric Power Research Institute of State Grid Chongqing Electric Power Company, Chongqing, China. His research interests include power system resilience and emergency resource scheduling.